Research Article

Journal of Environmental Nanotechnology

Effect of Manganese Doping in SnO_2 Thin Films and its NO_2 Gas Sensing Performance

R. Yogasaraswathi* and J. Dheepa

PG and Research Department in Physics, Government Arts College (Autonomous), Coimbatore, TN, India

Received: 02.10.2023 Accepted: 16.10.2023 Published: 30.12.2023

*yogasaraswathi.astro@gmail.com

ABSTRACT

By using an automated nebulizer spray pyrolysis technique with varied concentrations of manganese chloride (0 - 3%) in the spray solution of tin chloride, thin films of pure and manganese-doped tin oxides (Mn-SnO_2) were deposited. X-ray diffraction investigations indicated that 2% Manganese chloride concentration in the spray solution promoted development along (200) and (220) directions. The preferred growth direction in the (200) and (220) planes decreased with increasing manganese chloride doping concentration (2-3%) in the solution. The surface morphology of the films had changed as a result of adding Manganese as a dopant. Compositional analysis was carried out using EDAX. From UV-Vis spectroscopy, the optical properties of the SnO_2 and Mn-SnO_2 thin film were observed; the maximum optical absorbance was in the wavelength range of 300 - 400 nm. The concentration of Mn in the films affected the intensity of the photoluminescence emission peak detected at 347 and 392 nm for pure SnO_2 and Mn-SnO_2 films, respectively. The gas sensing performance of the films was examined by dynamic method against NO_2 gas, at an operating temperature of 250 °C and 400 ppm gas concentration**.** Mn-SnO_2 films achieved quick response and recovery times of 17 s and 34 s.

Keywords: Manganese doping; Thin films; Gas sensing; SnO_2; NO_2.

1. INTRODUCTION

In most solid-state gas sensors, thin films of polycrystalline semiconducting metal oxide materials like SnO_2 are utilized (Kiruthiga *et al.* 2022; Lee *et al.* 2000; Wang *et al.* 2010; Yamazoe *et al.* 1983; Yamazoe and Miura, 1992). The development in the properties of these materials has been the main focus of studies done in this area till now. The gas sensitivity of polycrystalline semiconductor metal oxide materials might be improved in a variety of methods nowadays; doping and adding more metals are the most efficient methods for achieving those goals (Cheng *et al.* 2021; Vijendra *et al.* 2020; Wang *et al*. 2020). The surface reactivity, adsorption and desorption characteristics of gas-sensing materials can be successfully modified by these metals, which are efficient catalysts. It was discovered that adding transition metals having the properties of noble metals to a gas sensing system can improve sensor response and selectivity, and help to increase sensitivity, reduce operating temperatures and other factors (Navale *et al.* 2021; Dayekh and Hussain, 2023; Basu and Basu, 2009; Ze *et al.* 2022). In addition, transition metals including Mn, Zn, Fe, W, Ni, Co, and Cr are excellent catalysts (Saruhan *et al.* 2021; Tomatis *et al.* 2018). According to research, adding transition metals as doping agents or even as an addition layer also enables modifying the electro-physical characteristics, structural characteristics, catalytic activity and adsorption characteristics of the doped and added material (Navale *et al.* 2021; Dayekh and Hussain, 2023). Transition metals and metal oxides are therefore frequently used as catalysts in heterogeneous catalysis as well as doping components in the production of semiconductors (Korotcenkov *et al.* 2004; Lichen *et al.* 2018; Kanan *et al.* 2009). Even though transition metals have the potential to functionalize metal oxide characteristics that are essential in gas sensor applications, they are still used more rarely in gas sensors as transition metals (Choi *et al.* 2004; Kumar *et al*. 2009; Buvailo *et al*. 2010; Liua *et al.* 2010; Liu *et al.* 2015). Additionally, there is insufficient depth in the research on the gas-sensing characteristics of metal oxides doped with transition metals. An attempt has been made in this work to deal with initial changes in dopant to observe the performance of doped SnO_2 film for further research development.

2. EXPERIMENTAL DETAILS

Tin oxide films and manganese-doped tin oxide films were deposited using tin dichloride dihydrate ($SnCl_2{\cdot}2H_2O$) and manganese chloride ($MnCl_2$), respectively. Double-distilled water and ethanol were mixed in a 3:1 combination. In this mixture, an accurately determined quantity of $SnCl_2{\cdot}2H_2O$ was added to create the precursor solution, which had a strength of 0.3 M. Then, the mixture was stirred in a magnetic stirrer until it became a clear precursor solution; subsequently, it was first transferred into a solution holder and then sprayed onto the hot substrate kept at the deposition temperature

of 450 °C using a thermocouple-based digital temperature controller. For manganese-doped tin oxide film, additionally, manganese chloride was added in ethanol, distilled water and tin dichloride mixture (Palanichamy *et al.* 2019; Mariappan *et al.* 2013; Kumar *et al.* 2017) with different doping percentages. The spray rate of the solution to the hot substrate was maintained at 0.1 ml/min throughout the experiment, the distance between the spray nozzle and the substrate was set at 10 cm, the pressure of the carrier gas was held at 0.2 Pa for both films and the coating volume was kept constant at 5 ml. After deposition, films were permitted to gradually cool at room temperature (Tamil *et al.* 2016).

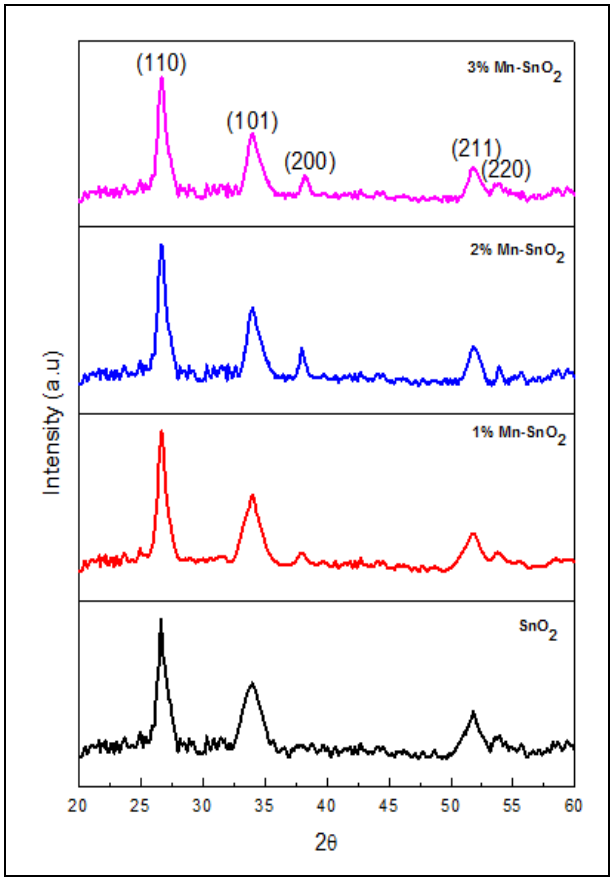

Fig. 1: XRD pattern of Pure SnO_2 and Mn-SnO_2 thin films

3. RESULTS AND DISCUSSION

3.1 X-RAY DIFFRACTION ANALYSIS

Fig. 1 depicts the XRD patterns of pure and different percentages of manganese-doped SnO_2 thin films. The JCPDS cards were used to identify the individual peaks, which are located at 2θ = 26.6°, 33.89°, 37.95°, 51.78° and 54.75°, respectively, with (h k l) values of (110), (101), (200), (211) and (220). The polycrystalline tetragonal rutile-type SnO_2 phase is observed in both instances, and the peak locations of the films are discovered to be in excellent agreement with JCPDS data card 41-1445. A strong influence on the structural properties was observed when the doping concentration of Mn was increased as 2% in Mn-SnO_2 film. It was confirmed by the variation of diffraction pattern intensity.

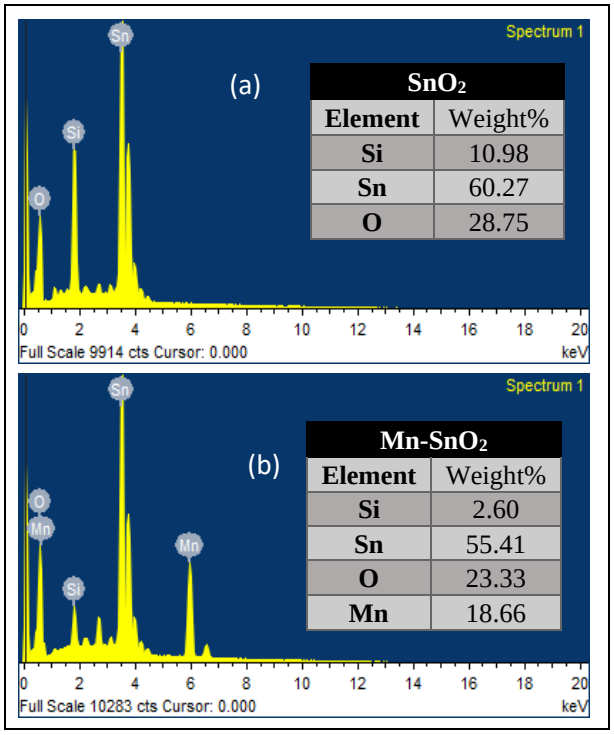

Fig. 2: (a & b) EDAX spectra of Pure and Mn-doped SnO_2 thin films

The particle size ranges between several nanometers. The determined grain size is shown in Table 1, and the FWHM of the diffracted peak was used to determine the strain and particle size.

The following equation was used to compute the lattice constants and average particle size (D) (Zoleikha *et al.* 2022),

$$D = \frac{k\lambda}{\beta \cos\theta} \quad \ldots\ldots\ldots\ldots\ldots (1)$$

$$\frac{1}{d^2} = \frac{h^2+k^2}{a^2} + \frac{l^2}{c^2} \quad \ldots\ldots\ldots\ldots (2)$$

where, d is the interplanar spacing, θ is the Bragg diffraction angle, β is the full width at half maximum (FWHM), and λ is the X-ray wavelength, which has a value of 1.542. The crystallite size is in the range of several nanometers according to Scherrer's equation. The following equations have been used to determine the lattice strain (ε) and dislocation density (δ) of pure and Mn-doped SnO_2 thin films (Vinila *et al.* 2022; Said *et al.* 2018),

$$\varepsilon = \frac{\beta}{4\tan\theta} \ldots\ldots\ldots\ldots (3)$$

$$\delta = \frac{1}{D^2} \ldots\ldots\ldots\ldots\ldots (4)$$

In Table 1, the estimated values for the micro-structural parameters are given. Although the data in Table 1 for pure and different doping concentrations indicate different particle sizes, they are all at the nanoscale level. It further demonstrates that the value of dislocation density and strain for the various doping concentrations is due to an increase in the number of defects, which is favorable for gas sensing (Maheswari *et al*. 2020).

The c/a ratio for pure SnO_2 and Mn-doped SnO_2 films was found to increase (Table 1) up to 2% of Mn doping. Depending on the ionic radius and crystallinity of the dopant, the rise in lattice constant may result from an increase in the doping percentage of elements up to 2%, which will impact the original structure. As a result, there is a noticeable rise in the lattice constant, which supports the inclusion of the ions in the host lattice.

3.2 ELEMENTAL ANALYSIS

The quantitative analysis of the prepared thin films was carried out to determine the elemental composition between pure SnO_2 and Mn-SnO_2 films. Fig. 2 (a & b) shows the film composition which confirms the presence of Sn, O and Mn peaks in corresponding samples. The presence of silicon in the films was because of the usage of the glass substrate.

3.3 MORPHOLOGICAL STUDY

The surface morphology of the prepared films was analyzed by using a Field Emission Scanning Electron Microscope (FE-SEM) with ~5 K to ~100 K magnifications which are shown in Fig 3(a) to (b).

The particles were uniformly distributed with good surface coverage, had good crystallinity and a high magnification image revealed the presence of flax-like grains in pure SnO_2 film; whereas, Mn-SnO_2 film was seemingly found to have evenly coated spherical grains.

3.4 OPTICAL CHARACTERIZATION

The relationship between optical absorption and photon energy for films sprayed with a nebulizer atomizer is shown in Fig. 4. The films exhibit a rise in absorbance at wavelengths above 250 nm. The maximum absorbance intensity of the deposited films was recorded at the wavelength range from 315 nm to 350 nm.

Tauc plot was used to estimate the optical band gap energy (E_g). The optical absorption coefficient at the absorption edge for direct inter-band transition is given by,

$$(\alpha h\nu)^2 = A\,(h\nu - E_g) \quad \ldots\ldots\ldots (5)$$

where, A is the absorption constant for a direct transition, h is Planck's constant, ν is photon frequency and E_g is the optical band gap. (Kamble *et al*. 2017).

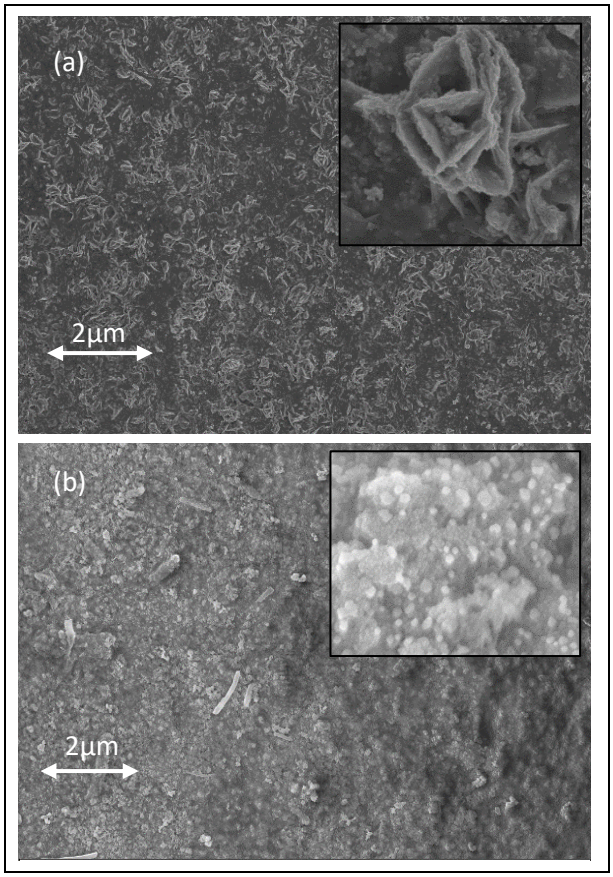

Fig. 3: (a & b) FESEM image of pure and Mn-SnO_2 thin films

By plotting $(\alpha h\nu)^2$ vs. hν (inset of Fig. 4), the band gap for a direct allowed transition was determined. At ambient temperature, the UV band gap values of deposited films were 3.44 eV for pure SnO_2 and 3.23, 3.17 and 3.25 eV for Mn-doped SnO_2 films with concentrations of 1, 2 and 3%, respectively. Due to a reduction in particle size on Mn-SnO_2 thin films, the band gap value seemingly decreased for 1 and 2% of Mn-doped SnO_2 films (Aboud *et al*. 2019).

3.5 PHOTOLUMINESCENCE PROPERTIES

Photoluminescence (PL) measurement at room temperature was adopted to ensure the optical properties and the possible effect of Mn incorporation in doped SnO_2 films. Fig. 5 depicts the PL spectra of pure SnO_2 and Mn-SnO_2 thin film, which has the highest peak emission intensity wavelength at 347 nm and 392 nm for both pure and Mn-doped SnO_2 films as the excitation source with broad visible emission range from 325 - 450 nm. Due to the increase in oxygen vacancies in the Mn-doped SnO_2 film, the PL peak intensity increased for 0-2% Mn concentration. As a result of the decrease in grain size, the oxygen vacancy ratio increased in the

manufactured Mn-doped SnO_2 thin film, which raised the PL intensity of the doped films (Azam *et al.* 2012).

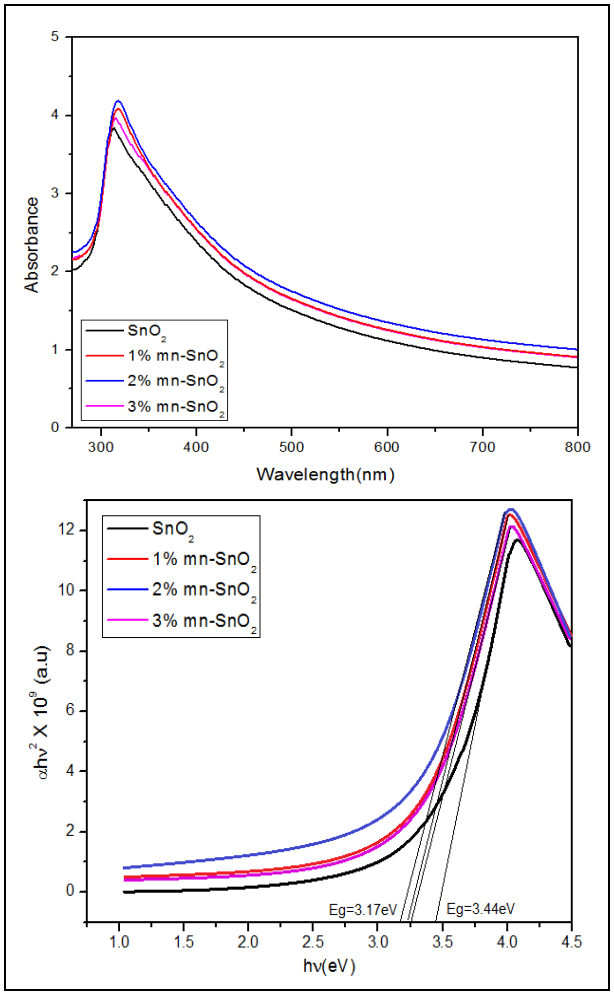

Fig. 4: UV-Vis spectra of Pure and Mn-SnO_2 thin films

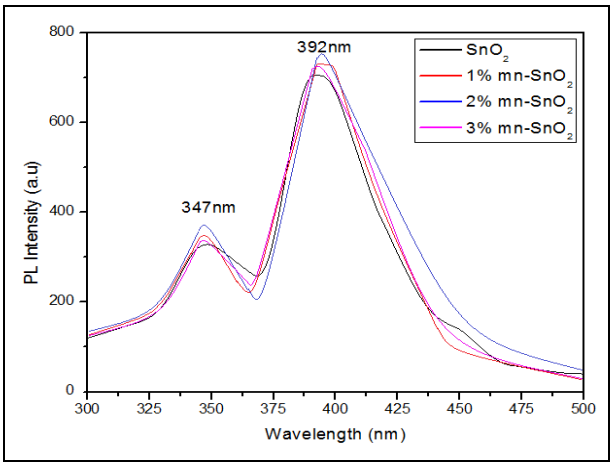

Fig. 5: PL spectra of Pure and Mn-SnO_2 thin films

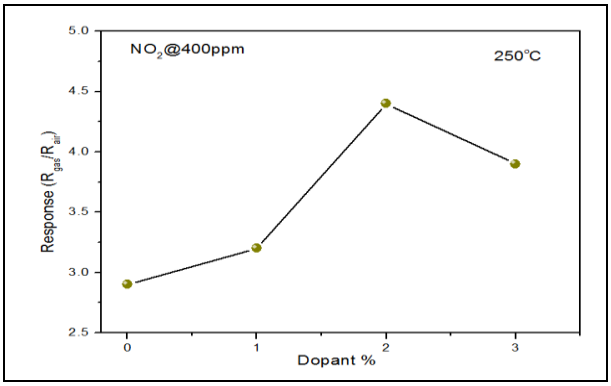

Fig. 6: Response graph of 0-3% Mn-SnO_2 thin films

3.6 SENSOR RESPONSE

The dynamic gas sensing assembly carried out the investigations on the gas response of pure and Mn-doped SnO_2 thin films against NO_2 gas at operating temperatures of 250 °C in 400 ppm of gas concentration. The semiconducting thin-film metal oxide gas sensors were deeply investigated (Guan *et al*. 2020).

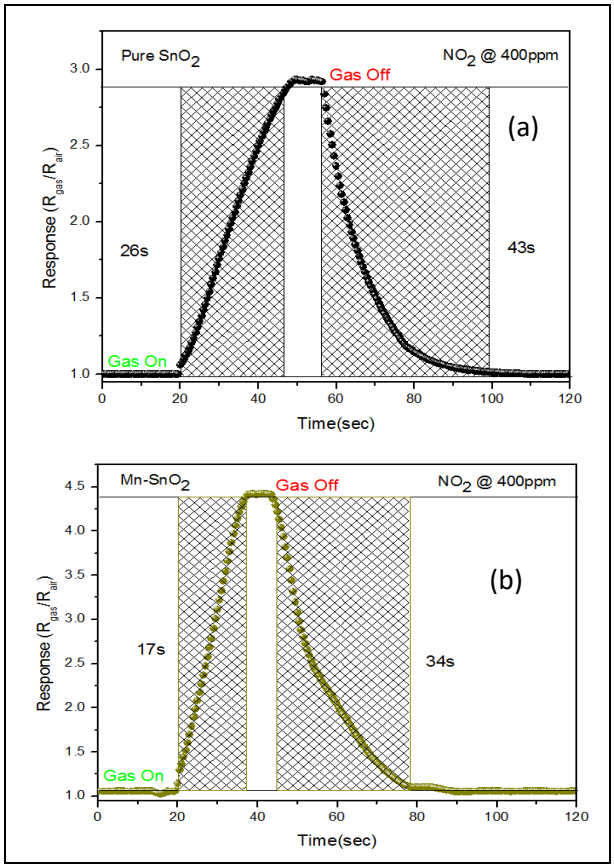

Fig. 7: (a & b) Response and recovery time of Pure and Mn-SnO_2 thin films towards NO_2 gas

The gas response is influenced by factors including structure, concentrations, film thickness, morphology and operating temperatures. In this present work, the gas response towards NO_2 gas for pure SnO_2 and Mn-doped SnO_2 thin films was examined. The response graph of SnO_2 films doped with 0-3% Mn is shown in Fig. 6. However, 2% Mn-doped SnO_2 thin film exhibited an impressive reaction towards NO_2 gas with 400 ppm of gas concentration when operated at 250 °C. It has been discovered that when compared to pure SnO_2, 2% Mn-SnO_2 exhibited a stronger sensitivity towards NO_2 gas (Salah *et al*. 2020).

Table 1. Calculated grain sizes of SnO_2 and Mn-SnO_2 thin films

Name of the thin film samples	Lattice Constant(Å)		Thickness of the film (µm)	Particle size (nm)	Dislocation Density (x 10^{15}) lines. m^{-2}	Strain ($\times10^{-3}$)
	a	c				
SnO_2	4.7031	3.1733	119.5	56.66	0.312	20.21
1%Mn-SnO_2	4.7044	3.1773	120	55.13	0.329	20.43
2%Mn-SnO_2	4.7110	3.1802	120	42.02	0.566	24.65
3%Mn-SnO_2	4.7093	3.1781	120	43.32	0.533	22.37

Table 2. NO_2 gas sensing performances of various SnO_2-based thin films

Material	Fabrication method	Op. temperature/NO_2 concentration	Response	t_{res}/t_{rec}	Reference
"SnO_2 –NiO	"Sputtering	"200°C/10 ppm	"2.25 (Rg/Ra)	-	(Jose *et al.* 2020)
SnO_2 –MoO_3	Sol –gel	170°C/500 ppm	3.75 ((Rg −Ra)/Ra)	2s/ -	(Kaur *et al*. 2010)
SnO_2 –In_2O_3	FSP method	250°C/50 ppm	~3 (Rg/Ra)	2s/3mns	(Inyawilert *et al*. 2015)
SnO_2 –SnO	Sputtering	60°C/10 ppm	4.35 ((Ig −Ia)/Ia)	165s/329s	(Jeong *et al*. 2018)
SnO_2 –Ag_2O"	Sputtering"	275°C/10 ppm"	5.91 (Rg/Ra)"	28s/168s	(Yuan *et al*. 2022)
SnO_2:WO_3	Thermal evaporation	250ºC/220ppm	~550 ((R_g-R_a)/R_a)	2s/120s	(Haidar *et al*. 2018)
Zn_2SnO_4	Spray pyrolysis	200 ºC /200ppm	3.31 (Rg/Ra)	25s/221s	(Ganbavle *et al*. 2014)
$ZnSnO_3$	Spray pyrolysis	RT/80ppm	12.05 ((R_g-R_a)/R_a)	169s/217s	(Dabbabi *et al*. 2019)
CdS-SnO_2	Chemical Solution Deposition	RT/10ppm	377.7 (Rg/Ra)	8s/107s	(Ajay *et al*. 2022)
SnO_2-Pd	Flame Chemical Vapor Deposition	30ºC/10ppm	12.35 (Rg/Ra)	~300s/750s	(Myung *et al*. 2021)
B-doped CNTs/SnO_2	CVD	RT/500ppb	0.91 ((R_g-R_a)/R_a)	1min/2.5hours	(Leghrib *et al*. 2011)
Ni- SnO_2	Electrospinning	200 ºC/20 ppm	180.7 (Rg/Ra)	24 s /35 s	(Wen *et al*. 2017)
Ag-SnO_2/rGO	Sol-gel	RT /50ppm	2.13 (Ra/Rg)	35s/ -	(Wenqian *et al*. 2021)
Sb-doped Zn_2SnO_4	Sputtering	600ºC/300ppm	4 (Rg/Ra)	-	(Yamada *et al*. 1998)
Mn-SnO_2	Automated Nebulizer Spray Pyrolysis	250ºC/400ppm	4.4 (Rg/Ra)	17s/34s	This work

3.7 RESPONSE AND RECOVERY TIME

Fig. 7 (a & b) displays the response and recovery time of pure and Mn-SnO_2 thin films for 400 ppm of NO_2 gas at 250 °C. It has been noted that the Mn-SnO_2 thin film sensor responded to NO_2 gas at a maximum time of 17 s and recovered in 34 s, owing to the presence of a doping element with a good percentage (Sureshkumar *et al.* 2019). For pure SnO_2 film, 26 s and 43 s of response and recovery times were observed, respectively.

Table 2 can be used to compare the gas response results of the present investigation against the results of other investigations. The sensor performance results in the current work demonstrated an improvement in rapid response and recovery times and sensor response value. The optimal doping percentage is realized as the response reached 4.4 at 400 ppm of NO_2 gas with very quick response and recovery times of 17 s and 34 s, respectively. This illustrates that 2% of Mn-doped SnO_2 thin film has great potential to be a promising NO_2 gas sensor.

4. CONCLUSION

Using an automated nebulizer spray pyrolysis technique, thin films of pure SnO_2 and Mn-SnO_2 were deposited on the glass substrate. XRD, EDAX, FESEM, UV-visible spectroscopy, PL characteristics and gas sensor performance were used to characterize the prepared thin films. The XRD spectra of all samples exhibited tetragonal rutile-type SnO_2 phases, and the peak position of the films was found to be in good match with JCPDS data. Due to doping, the average crystallite size decreased. The homogeneous dense nanoparticles that developed on the substrate were seen in the FE-SEM image of the pure and Mn-SnO_2 thin films. As compared to pure SnO_2 thin films, the band gap energy values for Mn-SnO_2 thin films were lower. The concentration of doping affects the PL intensity. 2% Mn-doped SnO_2 thin film has shown the strongest response to NO_2 gas at a working temperature of 250 °C, as well as a quick reaction and rapid recovery times. Therefore, it might be concluded that Mn-SnO_2 thin films would be effective NO_2 gas sensors. The focus shall be laid upon 2% Mn-SnO_2 films for further research of SnO_2-based thin film works.

FUNDING

This research received no specific grant from any funding agency in the public, commercial or not-for-profit sectors.

CONFLICTS OF INTEREST

The authors declare that there is no conflict of interest.

REFERENCE

Aboud, A. A., Mukherjee, A., Revaprasadu, N. and Mohamed, A. N., The effect of Cu-doping on CdS thin films deposited by the spray pyrolysis technique, *J. Mater. Res. Technol.*, 8(2), 2021–2030 (2019). https://doi.org/10.1016/j.jmrt.2018.10.017

Ajay, K. S., Jatinder, P. S., Babita, S., Sandeep, M., Anjali, S., Monika, T. and Arijit, C., CdS-SnO2 nanocomposite sensor for room temperature detection of NO2 gas, *Sens. Technol*., 886, 283–289 (2022). https://doi.org/10.1007/978-3-030-98886-9_22

Azam, A., Ahmed, A. S., Habib, S. S. and Naqvi, A. H., Effect of Mn doping on the structural and optical properties of SnO_2 nanoparticles, *J. Alloys Compd.*, 523, 83-87 (2012). https://doi.org/10.1016/j.jallcom.2012.01.072

Basu, S. and Basu, P. K., Nanocrystalline Metal Oxides for Methane Sensors: Role of Noble Metals, *J. Sens*., 2009, 1-20 (2009). https://doi.org/10.1155/2009/861968

Buvailo, A. I., Oleksenko, L. P. Maksimovich, N. P., Matushko, I. P., Ripko, A. P., Ruchko, V. P., Effect of SnO2 particle size on the hydrogen sensitivity of adsorption – semiconductor sensors with CoxOy/SnO2 active coating, *Theor. Exp. Chem*., 46(3), 153–157 (2010). http://dx.doi.org/10.1007/s11237-010-9132-3

Cheng, P., Wang, Y., Wang, C., Ma, J., Xu, L., Lv, C., Sun, Y., Investigation about doping effects of different noble metals for ethanol gas sensors based on mesoporous In_2O_3, *Nanotechnol.*, 32(30), 305503 (2021). https://doi.org/10.1088/1361-6528/abf453

Choi, U. S., Sakai, G., Shimanoe, K. and Yamazoe, N., Sensing properties of SnO_2–Co_3O_4 composites to CO and H_2, *Sens. Actuators, B*, 98(1-2), 166–173 (2004). http://dx.doi.org/10.1016/j.snb.2003.09.033

Dabbabi, S., Nasr, T. B., Madouri, A., Cavanna, A., Garcia-Loureiro, A., and Kamoun, N., Fabrication and Characterization of Sensitive Room Temperature NO2 Gas Sensor Based on ZnSnO3 Thin Film, *Phys. Status Solidi A*, 216(16), 1-6 (2019). https://doi.org/10.1002/pssa.201900205

David, D., Udo, W. and Nicolae, B., Current Understanding of the Fundamental Mechanisms of Doped and Loaded Semiconducting Metal-Oxide-Based Gas Sensing Materials, *ACS Sens*., 4(9), 2228-2249 (2019). https://doi.org/10.1021/acssensors.9b00975

Dayekh, M. L. and Hussain, S. A., Gas Sensor and Sensitivity, *IntechOpen*, Chapter 1 (2023). https://doi.org/10.5772/intechopen.108040

Ganbavle, V., Patil, M. A., Deshmukh, H. P., Rajpure, K. Y., Development of Zn2SnO4 thin films deposited by spray pyrolysis method and their utility for NO2 gas sensors at moderate operating temperature, *J. Anal. Appl. Pyrolysis*, 107, 233-241 (2014). https://doi.org/10.1016/j.jaap.2014.03.006

Guan, W., Tang, N., He, K., Hu, X., Li, M. and Li, K. Gas-Sensing Performances of Metal Oxide Nanostructures for Detecting Dissolved Gases: A Mini Review, Front. Chem., 8, 1-5 (2020). https://doi.org/10.3389/fchem.2020.00076

Haidar, J. A. A., Muthafar, F. A. H. and Mohammed, K. K., Comparative NO2 Sensing Characteristics of SnO2:WO3 Thin Film Against Bulk and Investigation of Optical Properties of the Thin Film, *Baghdad Science Journal*, 15(2), 227-233 (2018). https://doi.org/10.21123/bsj.2018.15.2.0227

Inyawilert, K., Wisitsoraat, A., Sriprachaubwong, C., Tuantranont, A., Phanichphant, S. and Liewhiran, C., Rapid ethanol sensor based on electrolytically -exfoliated graphene –loaded flame -made In -doped SnO2 composite film, *Sens. Actuators B Chem*., 209, 40-55 (2015). https://doi.org/10.1016/j.snb.2014.11.086

Jeong, H. S., Park, M. J., Kwon, S. H., Joo, H. J., Song, S. H., Kwon, H. I., Low temperature NO2 sensing properties of RF-sputtered SnO SnO2 heterojunction thin -film with p -type semiconducting behavior, *Ceram. Int.*, 44(14), 17283-17289 (2018). https://doi.org/10.1016/j.ceramint.2018.06.189

Jose, A. S., Prajwal, K., Chowdhury, P. and Barshilia, H. C., Sputter deposited p -NiO/n -SnO2 porous thin film heterojunction based NO2 sensor with high selectivity and fast response, *Sens Actuators B Chem*., 310, 1-10 (2020). https://doi.org/10.1016/j.snb.2020.127830

Kamble, D. L., Namdev, S. H., Patil, V. L., Patil, P. S., and Kadam, L. D., Characterization and NO_2 gas sensing properties of Spray Pyrolyzed SnO_2 Thin Films, *J. Anal. Appl. Pyrolysis*, 127, 38-46 (2017). https://doi.org/10.1016/j.jaap.2017.09.004

Kanan, S. M., El-Kadri, O. M., Abu-Yousef, I. A. and Kanan, M. C., Semiconducting Metal Oxide Based Sensors for Selective Gas Pollutant Detection, *Sens.*, 9(10), 8158-8196 (2009). https://doi.org/10.3390/s91008158

Kaur, J., Vankar, V. D. and Bhatnagar, M. C., Role of surface properties of MoO_3-doped SnO2 thin films on NO2 gas sensing, *Thin Solid Films*, 518(14), 3982-3987 (2010). http://dx.doi.org/10.1016%2Fj.tsf.2009.11.016

Kiruthiga, G., Rajni, K.S., Geethanjali, N., Raguram, T., Nandhakumar, E. and Senthilkumar, N., SnO_2: Investigation of optical, structural, and electrical properties of transparent conductive oxide thin films prepared by nebulized spray pyrolysis for photovoltaic applications, *Inorg. Chem. Commun*., 145, 109968 (2022). https://doi.org/10.1016/j.inoche.2022.109968

Korotcenkov, G., Macsanov, V., Brinzari, V., Tolstoy, V., Schwank, J., Cornet, A. and Morante, J., Influence of Cu, Fe, Co, and Mn oxide nanoclusters on sensing behavior of SnO_2 films, *Thin Solid Films*, 467(1-2), 209-214 (2004). https://doi.org/10.1016/j.tsf.2004.03.028

Kumar, K. D. A., Valanarasu, S., Jeyadheepan, K., Hyun-Seok K. and Dhanasekaran, V., Evaluation of the physical, optical, and electrical properties of SnO2: F thin films prepared by nebulized spray pyrolysis for optoelectronics, *J. Mater. Sci: Mater. Electron*., 29, 3648–3656 (2017). https://doi.org/10.1007/s10854-017-8295-2

Kumar, V., Srivastava, S. K., Kiran, J., Cobalt doped SnO2 thick film gas sensors: conductance and gas response characteristics for LPG and CNG gas, *Sensors and Transducers Journal*, 101(2), 60–72 (2009).

Lee, S., Tsai, P. and Chen, H., Comparison study of SnO2 thin- and thick-film gas sensors, *Sens. Actuators, B*, 67(1-2), 122-127 (2000). https://doi.org/10.1016/S0925-4005(00)00390-7

Leghrib, R., Felten, A., Pireaux, J. J. and Llobet, E., Gas sensors based on doped-CNT/SnO2 composites for NO2 detection at room temperature, *Thin Solid Films*, 520(3), 966-970 (2011). https://doi.org/10.1016/j.tsf.2011.04.186

Lichen, L. and Avelino, C., Metal Catalysts for Heterogeneous Catalysis: From Single Atoms to Nanoclusters and Nanoparticles, *Chem. Rev.*, 118(10), 4981-5079(2018). https://doi.org/10.1021/acs.chemrev.7b00776

Liu, C., Kuang, Q., Xie, Z. and Zheng, L., The effect of noble metal (Au, Pd, Pt) nanoparticles on the gas sensing performance of SnO2-based sensors: a case study on the {221} high-index faceted SnO2 octahedra, *Cryst. Eng. Comm*., 17(33), 6308-6313 (2015). https://doi.org/10.1039/C5CE01162K

Liua, L., C. Guo, S. Li, L. Wang, Q. Dong, W. Li, Improved H2 sensing properties of Co-doped SnO2 nanofibers, *Sens. Actuators, B*, 150, 806-810 (2010). https://doi.org/10.1016/j.snb.2010.07.022

Maheswari, S., Karunakaran, M., Kasirajan, K., Bruno, C. L., Boomi, P., Yttrium - Substituted SnO_2 thin films and its gas sensing activity against NH_3 gas: Characterization and sensitivity evaluation, *Sens. Actuators, A*, 315, 1-10 (2020). https://doi.org/10.1016/j.sna.2020.112303

Mariappan, R., Ponnuswamy, V., Suresh, P., Suresh, R., Ragavendar, M. and Sankar, C., Deposition and characterization of pure and Cd doped SnO2 thin films by the nebulizer spray pyrolysis (NSP) technique, *Mater. Sci. Semicond. Process.*, 16(3), 825-832 (2013). https://doi.org/10.1016/j.mssp.2013.01.006

Myung, S. C., Ali, M., Han, G. N., Sangwoo, K., Dong, E. K., Kyu, H. L., Changhyun, J. and Sun, W. C., Facile and fast decoration of SnO2 nanowires with Pd embedded SnO2-x nanoparticles for selective NO2 gas sensing, *Sens. Actuators, B*, 340, 1-14(2021). https://doi.org/10.1016/j.snb.2021.129984

Navale, S., Shahbaz, M., Mirzaei, A., Kim, S. S. and Kim, H. W., Effect of Ag Addition on the Gas-Sensing Properties of Nanostructured Resistive-Based Gas Sensors: An Overview, *Sens.*, 21(19), 6454 (2021). https://doi.org/10.3390/s21196454

Navale, S., Shahbaz, M., Mirzaei, A., Kim, S. S., Kim, H. W., Effect of Ag Addition on the Gas-Sensing Properties of Nanostructured Resistive-Based Gas Sensors: An Overview, *Sensors, 21(19)*, 1-28 (2021). https://doi.org/10.3390/s21196454

Palanichamy, S., Raj, M. J., Deva, A. K. K., Satheesh, K. P. S., Pandiarajan, S., Amalraj, L., Physical properties of rare earth metal (Gd3+) doped SnO2 thin films prepared by simplified spray pyrolysis technique using nebulizer, *Optik*, 194, 1-12 (2019). https://doi.org/10.1016/j.ijleo.2019.05.093

Said, N. D. M., Mohd, Z. S., Nafarizal, N., Hashim, S., Feri, A., Anis, S. B., Marlia, M., Difference in structural and chemical properties of sol–gel spin coated Al doped TiO_2, Y doped TiO_2 and Gd doped TiO_2 based on trivalent dopants, *RSC Adv*., 8(52) 29686–29697 (2018). https://doi.org/10.1039/C8RA03950J

Salah, E., Yasseen, K., Hadi, E, Chiad, S., Habubi, N., Haneen, K., Sensitivity of Nanostructured Mn-Doped Cobalt Oxide Films for Gas Sensor Application, *Nano Biomed. Eng.*, 12(3), 205-213 (2020). https://doi.org/10.5101/nbe.v12i3.p205-213

Saruhan, B., Lontio, F. R. and Nahirniak, S., Review: Influences of Semiconductor Metal Oxide Properties on Gas Sensing Characteristics, *Front. Sens*., 2, 1-24 (2021). https://doi.org/10.3389/fsens.2021.657931

Sureshkumar, S., Venkatachalapathy, B. and Sridhar, T M., Enhanced H2S gas sensing properties of Mn doped ZnO nanoparticles – an impedance spectroscopic investigation, *Mater. Res. Express*, 6(7), 1-22 (2019). https://doi.org/10.1088/2053-1591/ab0eef

Tamil, I. J., Rajalakshmi, P. and Oommen, R., Nebulized spray pyrolysis: a new method for synthesis of graphene film and their characteristics, *Surf. Coat. Technol*., 307, 65-72 (2016). https://doi.org/10.1016/j.surfcoat.2016.08.051

Tomatis, M., Xu, H., Wei, C., Bishop, M. T., He, J., Wang, C., Zhao, M., Xiao, H., Yu, H., Behera, S. N., Tang, B., A Comparative Study of Mn/Co Binary Metal Catalysts Supported on Two Commercial Diatomaceous Earths for Oxidation of Benzene, *Catal.*, *8(3)*, 1-22 (2018). https://doi.org/10.3390/catal8030111

Vijendra, S. B., Mirabbos, H., Mahesh, K., Enhanced sensing performance of ZnO nanostructures-based gas sensors: A review, *Energy Rep*., 6(4), 46-62(2020). https://doi.org/10.1016/j.egyr.2019.08.070

Vinila, V. S., Jayakumari, I., Synthesis and structural studies of superconducting perovskite GdBa2Ca3Cu4O10.5+δ nanosystems, *In Micro and Nano Technologies, Design, Fabrication, and Characterization of Multifunctional Nanomaterials, Elsevier*, 319-341 (2022). https://doi.org/10.1016/B978-0-12-820558-7.00022-4

Wang, C. N., Li, Y. L., Gong, F. L., Zhang, Y. H., Fang, S. M., Zhang, H. L., *Chem. Rec*., 20(12), 1553-1567 (2020**)**. https://doi.org/10.1002/tcr.202000088

Wang, C., Yin, L., Zhang, L., Xiang, D. and Gao, R., Metal oxide gas sensors: sensitivity and influencing factors, *Sens.*, 10(3), 2088-2106 (2010). https://doi.org/10.3390/s100302088

Wen, T. L., Xiao, D. Z. and Xin, G., Electrospun Ni-doped SnO2 nanofiber array for selective sensing of NO2, *Sens. Actuators*, *B*, 244, 509-521(2017). https://doi.org/10.1016/j.snb.2017.01.022

Wenqian, Y., Kunmeng, Z., Yi, C., Yanhan, L., Tao, D., Sheng, C., Xiaodong, S., NO2 detection and redox capacitance reaction of Ag doped SnO2/rGO aerogel at room temperature, *J. Alloys Compd*., 886, 1-9 (2021). https://doi.org/10.1016/j.jallcom.2021.161287

Yamada, Y., Seno, Y., Masuoka, Y., Yamashita, K., Nitrogen oxides sensing characteristics of Zn2SnO4 thin fim, *Sens. Actuators B - Chem*., 49(3), 248–252 (1998). https://doi.org/10.1016/S0925-4005(98)00135-X

Yamazoe, N. and Miura, N., Some basic aspects of semiconductor gas sensors, *Chem. Sens. Technol*., 4, 1942 (1992).

Yamazoe, N., Kurokawa, Y. and Seiyama, T., Effects of additives on semiconductor gas sensors, *Sens. Actuators*, 4, 283–289 (1983). https://doi.org/10.1016/0250-6874(83)85034-3

Yuan, C. L. and Yu, W. H., Design of thin-film configuration of SnO2–Ag2O composites for NO2 gas-sensing applications, *The Nanotechnology Reviews*, 11(1), 1842-1853 (2022). https://doi.org/10.1515/ntrev-2022-0111

Ze, W., Lei, Z. A., Jingzhao, W., Rui, Z., Pengfei, M., Jianan, W. and Wei, Y., Advances in functional guest materials for resistive gas sensors, *RSC Adv.*, 12(38), 24614-24632 (2022). https://doi.org/10.1039/D2RA04063H

Zoleikha, H., Reza, T. L., Fereshteh, R. A., 3 - Identification and analytical methods,Editor(s): Ali Maleki, In Micro and Nano Technologies, *Heterogeneous Micro and Nanoscale Composites for the Catalysis of Organic Reactions*, *Elsevier*, 33-51 (2022), https://doi.org/10.1016/B978-0-12-824527-9.00001-0